ISSN 0915-633X

NATIONAL INSTITUTE FOR FUSION SCIENCE

Turbulence Trigger for Neoclassical Tearing Modes in Tokamaks

S.-I. Itoh, K. Itoh and M. Yagi

(Received - Aug. 12, 2003)

NIFS-782 Sep. 2003

TOKI, JAPAN

Turbulence trigger for neoclassical tearing modes in tokamaks

Sanae-I. Itoh*, Kimitaka Itoh†, Masatoshi Yagi*

*Research Institute for Applied Mechanics, Kyushu University, Kasuga 816-8580, Japan
†National Institute for Fusion Science, Toki 509-5292, Japan

Abstract

Stochastic trigger by microturbulence for neoclassical tearing mode (NTM) is studied. NTM induces topological change of magnetic structure and has subcritical nature. It is found that the NTM can be excited regardless of the presence of seed islands. Transition rate of, probability density function for and statistically-averaged amplitude of NTM are obtained. Boundary in the phase diagram is determined as the statistical long time average of the transition conditions. NTM can be excited by crossing this boundary even in the absence of other global instabilities. The boundary is expressed in terms of the poloidal beta value. Its dependence on the ratio between the ion banana width and radius of the rational surface, ρ_b/r_s , is found to vary in the range of ρ_b/r_s and $(\rho_b/r_s)^2$, depending on the linear stability of the tearing mode.

PACS Index Category:
52.35.Py, 52.55.Th, 52.35.Ra, 52.35.Fa

Keywords:
neoclassical tearing mode, stochastic equation, turbulent noise, stochastic trigger, transition rate, probability density function, statistically-averaged amplitude, phase boundary, nonlinear MHD stabilization effect

I. Introduction

Magnetized plasmas are non-uniform and far from thermal equilibrium. Consequently, various kinds of bifurcations can appear [1,2] producing an abrupt change of the topological structure of the magnetic field. In tokamak and in other laboratory plasmas, such a process appears as a magnetohydrodynamic (MHD) instability named tearing mode [3,4]. It is associated with magnetic field reconnection. Global perturbations with wave vectors perpendicular to the magnetic field are unstable and, due to the plasma resistivity, they can develop radial components that break the field lines. An important problem is now investigated: the possibility of appearing such magnetic surface breaking in linearly stable, low resistivity plasmas.

One possible mechanism is a nonlinear instability, the neoclassical tearing mode (NTM) [5-7]. This is a subcritically excited tearing mode under the influence of the pressure gradient. The experiments have shown that such perturbations with finite amplitude become unstable even for parameters corresponding to linearly stable ones [8-10] and that they can be triggered by other global MHD instability (as the sawtooth) [10,11]. Nevertheless, in some experiments, the excitation of this instability occurred in the absence of the above triggers [11,12]. The onset conditions of the NTM are not yet clarified, although the suppression of this instability is necessary for stationary operation of high temperature plasma [13]. The NTM can be stochastically triggered in these conditions. The rate of stochastic transition was determined at thermal equilibrium by evaluating the potential barrier crossing induced by thermal fluctuations [14]. It is expected that in nonequilibrium and turbulent plasmas the transition is triggered by the turbulence noise but there is no theoretical prediction for the excitation rate of the NTM.

In this article, we formulate a Langevin equation for the NTM as a stochastic equation in the presence of noise source induced by background fluctuations. The statistical properties of NTM amplitude, such as the probability density function (PDF), the rate of excitation, the average of amplitude, the boundary in the phase diagram and its expression, are derived. We show that the stochastic excitation of NTM is possible to occur without a seed island if $\beta_p > \beta_{p*}$ holds. (β_p is the plasma pressure normalized to the poloidal magnetic field pressure, and β_{p*} is the boundary of the phase.) The dependence of β_{p*} on the ratio between the ion banana width and radius of the rational surface, ρ_b/r_s, is studied. It is found that the relation of β_{p*} to ρ_b/r_s varies in the rage between ρ_b/r_s and $(\rho_b/r_s)^2$, depending on the linear stability condition of the tearing mode.

We note that this mechanism is rather general. For instance, in fluid dynamics it explains the transition of a linearly stable system in a laminar state (flow in a pipe) to a self-sustained turbulent state [15]. The transition is triggered by random disturbances such as inlet conditions.

II. Model

2.1 Neoclassical tearing mode

2.1.1 Description of instability growth rate

The nonlinear instability of the NTM has been discussed, and a dynamical equation of Ohm's law was formulated for the evolution of the amplitude as a deterministic variable

$$\frac{1}{\eta}\frac{\partial}{\partial t}A + \Lambda[A]A = 0, \tag{1}$$

where

$$A \equiv \tilde{A}_* q^2 R/B r_s^3 q' \tag{2}$$

is the normalized amplitude of the (m, n) -Fourier component of helical vector potential perturbation $\tilde{A}_*$ at the mode rational surface, $r = r_s$, and $-\Lambda$ is the nonlinear growth rate ($-\Lambda > 0$ if unstable). The safety factor $q = rB/B_p R$ as a topological index satisfies the condition $q(r_s) = m/n$ at $r = r_s$. B is the main magnetic field strength, r and R are minor and major radii of torus, $q' = \mathrm{d}q/\mathrm{d}r$, and m and n are poloidal and toroidal mode numbers, respectively. The time is normalized to poloidal Alfven transit time,

$$\tau_{Ap} = qR/v_A \tag{3}$$

(v_A : Alfven velocity) and the length to r_s . The magnetic island width w , being normalized to r_s , is expressed as

$$w = A^{1/2}. \tag{4}$$

The coefficient η is the inverse of resistive diffusion time

$$\eta = \eta_{//}\mu_0^{-1} r_s^{-2} \tau_{Ap} = R_M^{-1}, \tag{5}$$

where $\eta_{//}$ stands for a parallel resistivity, and R_M is the Lundquist number (magnetic Reynolds number).

An explicit form of the growth rate is given by

$$-\Lambda = 2\Delta' A^{-1/2} - \frac{C_1}{W_1^2 + A^2} + \frac{C_2}{W_2 + A}, \tag{6}$$

within the neoclassical transport theory, where the first, second and third terms of RHS stand for the effects of current density gradient, polarization drift and bootstrap current, respectively. The term W_1 represents the cut-off due to the banana orbit effect [16], and we choose a simple model,

$$W_1 = \rho_b^2 r_s^{-2} . \tag{7}$$

W_2 represents the cut-off determined by the cross-field energy transport and is given as [17],

$$W_2 = \left(\frac{\chi_\perp}{\chi_\parallel}\right)^{1/2} \frac{1}{\varepsilon s n} . \tag{8}$$

where $\chi_\perp$ and $\chi_\parallel$ are thermal diffusivities perpendicular to and parallel to the magnetic field line, ε is the inverse aspect ratio, n is the toroidal mode number and $s = r_s q' / q$. (When the effect of the perpendicular diffusion is not effective, $\left(\chi_\perp/\chi_\parallel\right)^{1/2}/\varepsilon s n < \rho_b^2 r_s^{-2}$, W_2 is evaluated as $W_2 = \rho_b^2 r_s^{-2}$ [18].) Coefficient C_1 and C_2 are given as

$$C_1 = 2a_{\rm bs}\beta_{\rm p}\varepsilon^{1/2}\rho_b^2 r_s^{-2} L_q^2 L_p^{-2} \tag{9a}$$

and

$$C_2 = 2a_{\rm bs}\beta_{\rm p}\varepsilon^{1/2} L_q L_p^{-1} \tag{9b}$$

for the limit of small collisions [7,19-23], ρ_b is the banana width, L_q and L_p are the gradient scale lengths of safety factor and pressure, respectively, and $a_{\rm bs}$ is a numerical constant. (The coefficient C_2 includes weak dependence on collisionality. However, it is not included here.) In addition, the stabilization effect of good curvature of tokamaks is known [24], but is not kept in Eq.(6) explicitly. For a convenience to compare with the experimental results, above coefficients are rewritten as follows:

$$C_2 = \beta_{\rm p}/\beta_{\rm pn} \tag{10a}$$

with the normalizing poloidal beta value of

$$\beta_{\rm pn} = L_p/2a_{\rm bs}\varepsilon^{1/2} L_q , \tag{10b}$$

and

$$C_1 W_1^{-1} C_2^{-1} = b \equiv \left(\rho_b^2 r_s^{-2} W_1^{-1}\right) L_q L_p^{-1} \tag{11}$$

The parameter b is of the order of unity if one uses the condition $W_1 = \rho_b^2 r_s^{-2}$. β_{pn} is also of the order unity.

The parameter Δ' controls the linear stability criterion of tearing mode when induced by the current density gradient [3,4]. The tearing mode is linearly unstable (in the limit of $\beta_p = 0$) if

$$\Delta' > 0 \tag{12}$$

holds. Analyses on the nonlinear stabilization process have shown that the parameter Δ' decreases as the perturbation amplitude, A, grows. A simple formula

$$\Delta' = \Delta'_0 - h\sqrt{A} \tag{13}$$

has been found useful, and the coefficients Δ'_0 and h are determined by the current profile [25]. In the preceding article [26], this nonlinear stabilization term is neglected, for the simplicity of the argument. We here generalize the analysis for the case of $h \neq 0$.

2.1.2 Nonlinear instability

In the absence of the pressure gradient effects, the tearing mode is linearly unstable if $\Delta'_0 > 0$ holds, and the growth rate becomes smaller as the amplitude A becomes larger. The marginal stability condition $\Delta' = 0$ gives

$$\sqrt{A} = h^{-1} \Delta'_0 . \tag{14}$$

This shows a supercritical excitation of tearing mode across the critical condition $\Delta'_0 = 0$.

The neoclassical tearing mode, for which the plasma pressure gradient has both the stabilizing and destabilizing effects, can be nonlinearly unstable even if it is linearly stable. When the amplitude A takes finite values, $-\Lambda$ can be positive even if

$$\Delta' < 0 , \tag{15}$$

since C_1 and C_2 can be positive. Figure 1 illustrates the growth rate as a function of A for the case of $\Delta'_0 < 0$. The marginal stability condition $\Lambda = 0$ can have three solutions at

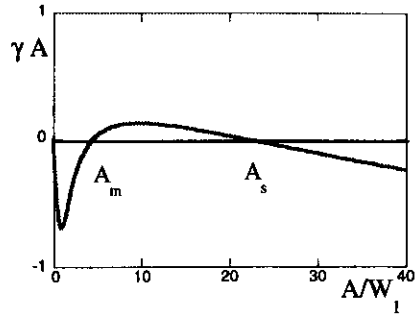

Fig.1 Normalized growth rate multiplied by amplitude, $\gamma A \equiv -\Lambda A/C_2$, is shown by solid line. Zeros indicate the nonlinear marginal stability conditions for the deterministic model. (Parameters are: $W_1 = W_2$, $C_1/2C_2W_1 = 1$, $h = 0$ and $\Delta'_0 W_1^{1/2}/C_2 = -0.0922$.)

$$A = A_0 \simeq 0 \ , \ A = A_m \ \text{and} \ A = A_s \tag{16}$$

($A_m < A_s$) if the parameter C_2 is large enough. In the range of amplitude

$$A_m < A < A_s \ , \tag{17}$$

the solution is not stable. That is, A_m and A_s are the threshold and saturation amplitudes of nonlinear instability, respectively.

2.1.3 Cusp catastrophe and subcritical excitation

The cusp catastrophe of the perturbation amplitude in the stationary state is expected in the deterministic model, because the marginal stability condition can have multiple solutions. The structure of the cusp is studied in this subsection.

From Eqs.(6) and (13), the marginal stability condition is rewritten as

$$\Delta'_0 = h\sqrt{A} + \frac{\sqrt{A}}{2}\frac{C_1}{W_1^2 + A^2} - \frac{\sqrt{A}}{2}\frac{C_2}{W_2 + A} \tag{18}$$

Near the linear stability boundary, $\Delta'_0 = 0$, A_m and A_s are estimated as follows. The balance between the second and third terms in the RHS of Eq.(18) gives an estimate of A_m as

$$A_m = C_1 C_2^{-1} = bW_1 \tag{19a}$$

and that between the first and third terms determines A_s as

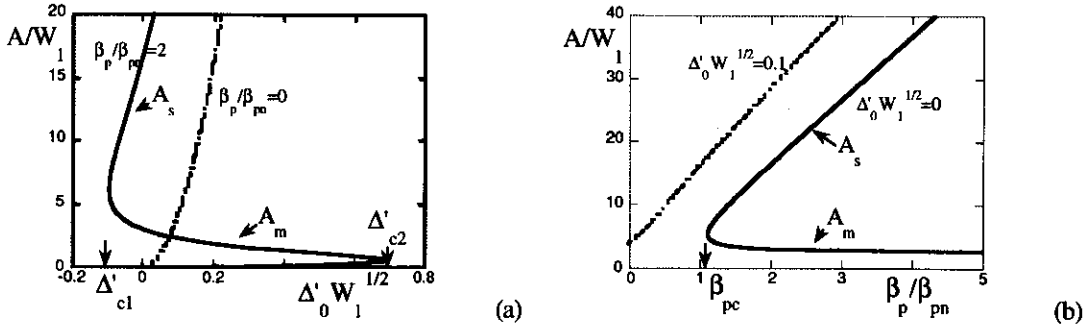

Fig.2 Marginal stability solutions $A = A_s$ and $A = A_m$. They are shown as a function of the linear MHD stability parameter Δ'_0 for fixed value of $\beta_p/\beta_{pn} = 2$ in (a). The limit of β_p=0 is also shown by the dotted line. (b) shows $A = A_s$ and $A = A_m$ as a function of β_p for fixed value of Δ'_0. The solid line shows the case of $\Delta'_0 = 0$, and the dashed line indicates the linearly unstable case $\Delta'_0 W_1^{1/2} = 0.1$. A_m in the linearly unstable case is not drawn in (b). (Other parameters are: $W_1 = W_2$, $C_1/2C_2W_1 = 1$, and $hW_1 = 1/20$.)

$$A_s = \frac{1}{2h} C_2 . \tag{19b}$$

Figure 2 illustrates the marginal stability condition. Amplitude A is shown as a function of Δ'_0 for the fixed value of β_p in Fig.2(a). In the presence of the pressure gradient (solid line), the subcritical excitation of the tearing mode is possible to occur. The dotted line is the result in the absence of the pressure gradient, $\beta_p = 0$, and the supercritical excitation takes place as is given as Eq.(14). Figure 2(b) shows the amplitude A_m and A_s as a function of β_p for the fixed value of Δ'_0. In Fig.2(b), the solid line shows the case of $\Delta'_0 = 0$, and the dashed line indicates the linearly unstable case $\Delta'_0 W_1 = 0.1$. Subcritical excitation appears in the linearly stable case.

Figure 2(a) shows that the equation $\Lambda = 0$ has multiple solutions in an intermediate parameter region,

$$\Delta'_{c1} < \Delta'_0 < \Delta'_{c2} \tag{20}$$

for given β_p. The cusp catastrophe of Fig.2(a) defines two ridge points, Δ'_{c1} and Δ'_{c2}. Δ'_{c1} and Δ'_{c2} are given by the local maximum and minimum of Eq.(18), respectively. One obtains an approximate estimate for asymptotic relations, by neglecting h, as

$$\Delta'_{c1} \simeq -\frac{C_2}{3\sqrt{3}\,b\,\sqrt{W_1}} = -\frac{1}{3\sqrt{3}\,b\,\sqrt{W_1}} \frac{\beta_p}{\beta_{pn}} \tag{21a}$$

and

$$\Delta'_{c2} \simeq 3^{-1/4}\left(\frac{3b}{4} - \frac{\sqrt{3}\,W_1}{2\left(1+\sqrt{3}\right)W_2}\right)\frac{1}{\sqrt{W_1}}\,C_2 \tag{21b}$$

This result demonstrates that the critical value of the stability parameter Δ'_0 is in proportion to β_p. The relation for the cusp ridge, Eq.(21a), is rewritten as that of β_p for the fixed value of Δ'_0. From Eq.(21a), the relation $\Delta'_0 = \Delta'_{c1}$ can be written as

$$\beta_p = \beta_{pc} \equiv 3\sqrt{3\,b}\,\beta_{pn}\sqrt{W_1}\left(-\Delta'_0\right). \tag{22}$$

for fixed negative value of Δ'_0. The ridge at $\beta_p = \beta_{pc}$ is denoted in Fig.2(b).

Owing to the nonlinear stabilization effect, the ridges of cusp, Δ'_{c1} and Δ'_{c2}, move forward the direction for increasing Δ'_0-value if $h \neq 0$. (The coefficient h denotes the magnitude of nonlinear stabilization effect of tearing mode as is defined Eq.(13).) Figure 3 illustrates the ridges of cusp, Δ'_{c1} and Δ'_{c2}, on the plane of $\left(\Delta'_0, \beta_p\right)$. The case of $hW_1 = 1/40$ is drawn by the solid line in Fig.3(a). The case of $h = 0$ is also shown by the dotted line, which shows the linear relations between Δ'_c and β_p as is expected from Eq.(21). The expanded view at the lower pressure gradient is illustrated in Fig.3(b). A critical point of the cusp appears in the low pressure gradient region. Below this critical point, the mode is subject to the supercritical excitation.

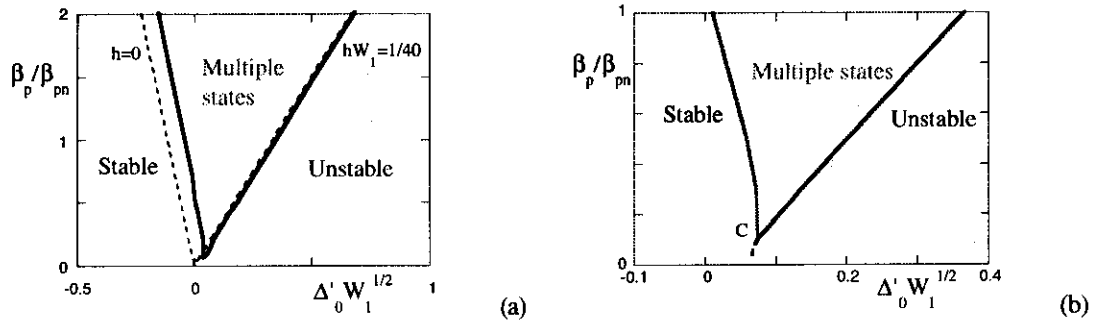

Fig.3 Ridge of cusp Δ'_{c1} and Δ'_{c2} on the plane of $\left(\Delta'_0, \beta_p\right)$. (a) illustrates the case of $hW_1 = 1/40$ (solid line), being compared with the case of $h = 0$ (dashed line). In the domain of "multiple states", the marginal stability condition has multiple solutions. (b) is the expanded view near the critical point of the cusp, $hW_1 = 1/40$. Dotted line is the boundary for the supercritical excitation. (Other parameters are: $W_1 = W_2$ and $C_1/2C_2W_1 = 1$)

2.2 Influence of microscopic fluctuations

The helical perturbation is subject to a random excitation from the micro turbulent noise. The level of noise is evaluated from the Lagrangian nonlinearity terms, and a stochastic equation is obtained instead of the deterministic equation (1)

$$\frac{\partial}{\partial t} A + \eta \Lambda A = s \frac{\delta^2}{a^2} \left[\phi_h, \Delta A_h\right]_k - s \left[\phi_h, A_h\right]_k - s \frac{v_{Te}}{v_A} \frac{\delta^2}{a^2} \left[A_h, \Delta A_h\right]_k , \qquad (23)$$

where $\delta = c/\omega_{pe}$ is the collisionless skin depth. ϕ_h is the stream function (normalized to $Ba^2\tau_{Ap}^{-1}$) and A_h is the vector potential of the microscopic turbulence [27]. The suffix h stands for the high mode numbers. The Poisson bracket $\left[u, v\right]$ is defined as $\left(\nabla u \times \nabla v\right) \cdot \boldsymbol{b}$, and $\boldsymbol{b} = \boldsymbol{B}/B$. $\left[\cdots\right]_k$ indicates the Fourier component that matches to the test macro mode, and k is the wave number for the macro mode.

We employ the following hierarchical approach. The microscopic turbulence has much shorter autocorrelation time τ_{ac} than that of the global perturbation. Both of micro and macro perturbations are statistically independent, and the adiabatic approximation is taken. Micro one is induced by plasma pressure gradient, and is considered to be in the nonlinearly marginal state [28]. The saturation levels ϕ_h and A_h can depend on A. We do not include such dependence here, but it can be introduced in the model.

2.2.1 Influence of coherent part

The RHS of Eq.(23) has two components. One is a coherent part, which has a fixed phase with respect to the global perturbation A. The coherent part is renormalized to turbulence-driven transport coefficients such as turbulent resistivity and viscosity. They would modify η, C_1 and C_2 [21-23]. For instance, $\eta_\parallel$ in Eq.(5) is affected to be

$$\eta_\parallel = \eta_{\parallel c} + \eta_N + \delta^2 r_s^{-2} \mu_e \qquad (24a)$$

where $\eta_{\parallel c}$ is the collisional resistivity, η_N is the turbulent resistivity, and μ_e is the electron viscosity owing to the turbulent diffusion. Turbulent viscosity μ_N and turbulent thermal diffusivity χ_N are also obtained by the similar renormalization procedure [1] and the global viscosity and thermal diffusivity are modified as

$$\mu = \mu_c + \mu_N \quad \text{and} \quad \chi = \chi_c + \chi_N . \qquad (24b)$$

The effect of polarization current may be modified. The stabilization term in Eq.(6) is evaluated as

$$C_1 \simeq \left(\frac{G_1 \omega_g \left(\omega_{*p} - \omega_g\right)\left(\omega - \omega_{*p}\right)}{\left(\omega - \omega_{*p} - \omega_g\right)\omega_{*p}^2} \frac{A}{W_1} - \frac{G_2\, \omega^2 \left(\omega - \omega_{*p}\right)^2}{\left(\omega - \omega_{*p} - \omega_g\right)^2 \omega_{*p}^2} \right) \beta_p \frac{\rho_b^2}{r_s^2} \frac{L_q^2}{L_p^2} \qquad (25)$$

where ω is the rotation frequency of the island in the plasma frame, ω_{*p} is the drift frequency defined by pressure gradient scale length, $\omega_{*p} = T/r_s eBL_p$, ω_g is the curvature drift frequency, $\omega_g = T/r_s eBL_M$ (L_M : scale length of magnetic field inhomogeneity) and G_1 and G_2 are numerical coefficients of the order unity [23]. The rotation frequency ω is determined by the turbulent viscosity and turbulent thermal conductivity. We note that the sign of C_1 and C_2 can change through this renormalization, Eq.(25). The electric induction by microfluctuations has been studied in conjunction with dynamo. The α–, β– and γ– dynamo have been known [1]. (Note that the first term in the parenthesis of Eq.(25) is related to the stabilizing term pointed out by Glasser et al. [29]. The magnetic well effect changes the linear stability boundary as well. This does not modify the qualitative feature of the cusp.) In this article, however, we use Eq.(6) and leave the other effects on Λ for future studies.

2.2.2 Influence of incoherent part

An incoherent part of RHS of Eq.(23), whose relative phase to A changes rapidly in time, contributes to the noise term. It is approximated to be random, i.e.,

$$\mathfrak{I}(t) = g\, w(t)\,, \qquad (26)$$

where g is the magnitude and $w(t)$ indicates white-noise.

2.3 Noise by microscopic turbulence

The noise term $\mathfrak{I}(t)$ has a quadratic form of ϕ_h and A_h, and the local instantaneous amplitude of $\mathfrak{I}(t)$ is estimated as

$$\left|\mathfrak{I}(t)\right| \simeq k k_h^3 C A_h^2\,; \qquad (27)$$

where numerical constant

$$C = -s f\left(\delta^2 r_s^{-2} + k_h^{-2}\right) + s\sqrt{\beta m_i/m_e}\,\delta^2 r_s^{-2} \qquad (28a)$$

with

$$f \equiv \phi_h / A_h \tag{28b}$$

is introduced. Estimations are made as

$$\Delta A_h = -k_h^2 A_h \quad \text{and} \quad \left| \nabla A_h \right| = k_h A_h \tag{29}$$

for microscopic turbulence, and as

$$\left| \nabla A \right| = k A \tag{30}$$

for macro test mode. k_h is the typical mode number of the micro fluctuations, the inverse of which is separated from the coherence length of macro mode. (For a case of ballooning mode turbulence in tokamaks, f is evaluated in ref.21 and is of the order unity.)

The statistical average $\sqrt{\langle g^2 \rangle}$ is related to $\left| \mathcal{J} \right|$ by the law of large numbers. Within the coherent area of global test mode, ℓk^{-1}, a large number

$$N = k_h^2 \ell k^{-1} \tag{31}$$

of independent kicks contribute to $\mathcal{J}(t)$. (ℓ : radial scale length of the macro mode. N is evaluated by noting a quasi-two-dimensional feature of fluctuations.) The average $\sqrt{\langle g^2 \rangle}$ is $N^{-1/2}$ times smaller than the instantaneous local value of $\left| \mathcal{J} \right|$. The magnitude g is evaluated as

$$g^2 = k\, k_h^{-2} \ell^{-1} \left| \mathcal{J} \right|^2 \tau_{ac} = \ell^{-1} k^3 k_h^4 C^2 A_h^4 \tau_{ac} , \tag{32}$$

having a dependence like $g^2 \propto \left(\tilde{B}_{r,h} / B_\theta \right)^4 \tau_{ac}$. Experimental magnitude is explained later.

III. Statistical solution

3.1 Stochastic equation and probability density function

The dynamical equation of NTM amplitude A, Eq.(23), is rewritten as a stochastic equation

$$\frac{\partial}{\partial t} A + \eta \Lambda A = g\, w(t) , \tag{33}$$

and A is now a stochastic variable.

The statistical property of the NTM amplitude A is studied. A schematic description of the solution of this stochastic equation is illustrated in Fig.4. The deterministic part of Eq.(33), ΛA , allows multiple metastable states. The random kick by the noise induces the barrier crossing, realizing the excitation and decay of the mode. In the long run, the most probable state is realized as a statistical average. It is worthwhile to compare it with Kramers' idea for thermal equilibrium [14]. In Eq.(33), there is a nonlinear force but no Einstein drag term common in Brownian theory; the fluctuations from turbulence are decidedly non thermal unlike standard Langevin theory.

The Fokker-Planck equation of $P(A)$ is deduced from Eq. (33) as

$$\frac{\partial}{\partial \tau} P + \frac{\partial}{\partial A}\left(\eta \Lambda + \frac{1}{2} g \frac{\partial}{\partial A} g\right) P = 0 \ . \tag{34}$$

The stationary solution of the PDF $P_{eq}(A)$ is expressed as

$$P_{eq}(A) \propto g^{-1} \exp\left(-S(A)\right) \tag{35}$$

by use of a nonlinear dissipation function as

$$S(A) = \int_0^A 2\eta \, \Lambda(A') g^{-2} A' \, dA' \tag{36}$$

which is proportional to the entropy production rate near the thermal equilibrium [1].

Using Eqs.(6) and (32), we have

$$S(A) = \Gamma\left(-\frac{4}{3}\Delta'_0 A^{3/2} + hA^2 + \frac{1}{2} C_1 \ln\left(1 + \frac{A^2}{W_1^2}\right) - C_2\left(A - W_2 \ln\left(1 + \frac{A}{W_2}\right)\right)\right) \tag{37}$$

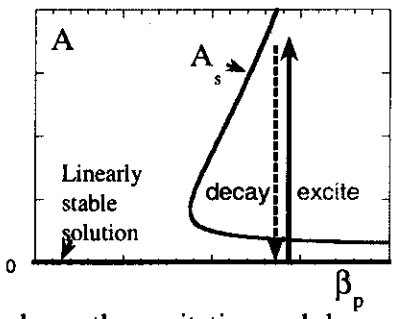

Fig.4 Schematic drawing that shows the excitation and decay of NTM perturbations owing to the turbulent noise.

with

$$\Gamma = 2\, R_M^{-1}\, \ell k^{-3} k_h^{-4}\, C^{-2}\, A_h^{-4} \tau_{ac}^{-1} \ . \tag{38}$$

The coefficient Γ shows a characteristic value of the ratio between the dissipation for crossing over the barrier and excitation by turbulence noise. Its magnitude and the parameter dependence are discussed at the end of this article.

Substituting Eq.(37) into Eq.(35), the PDF is given as

$$P_{eq}(A) \propto \exp\left(\Gamma \frac{4}{3} \Delta'_0 A^{3/2} - \Gamma h A^2 + \Gamma C_2 A\right)\left(1 + \frac{A^2}{W_1^2}\right)^{-\Gamma C_1/2}\left(1 + \frac{A}{W_2}\right)^{-\Gamma C_2 W_2} \tag{39}$$

The PDF has a stretched non-Gaussian exponential form with power-law dependence if $h = 0$. The exponential term is determined by the damping by current density gradient and the drive by bootstrap current. The power-law decay is mainly due to the polarization drift effect. The minimum of $S(A)$, i.e., zero of Λ, predicts the peak of PDF and the probable value of A .

3.2 Probable solutions

For the case of a bistable state, Eq.(20), two metastable states are allowed. The transition between them takes place, and the long time average describes the selection and partition rule between metastable states. The nonlinear potential $S(A)$ is shown in Fig.5 for the case of bistable state. Parameters are chosen in the linearly stable region, $\Delta'_0 < 0$, and $S(A)$ has two minima at

$$A = 0 \ \text{ and } A = A_s \ , \tag{40a}$$

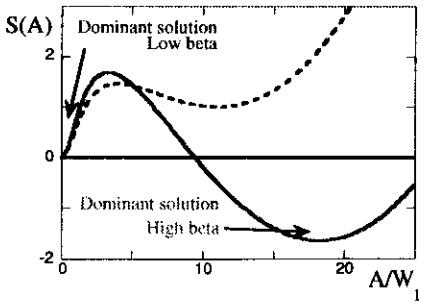

Fig.5 Nonlinear potential $S(A)$ (in the unit of ΓW_1) as a function of the perturbation amplitude for various values of beta: $\beta_p/\beta_{pn} = 1.2$ for dashed line, and $\beta_p/\beta_{pn} = 1.6$ for solid line. (Other parameters are: $\Delta'_0 W_1^{1/2} = -0.05$, $hW_1 = 1/40$, $W_1 = W_2$, and $C_1/2C_2W_1 = 1$.)

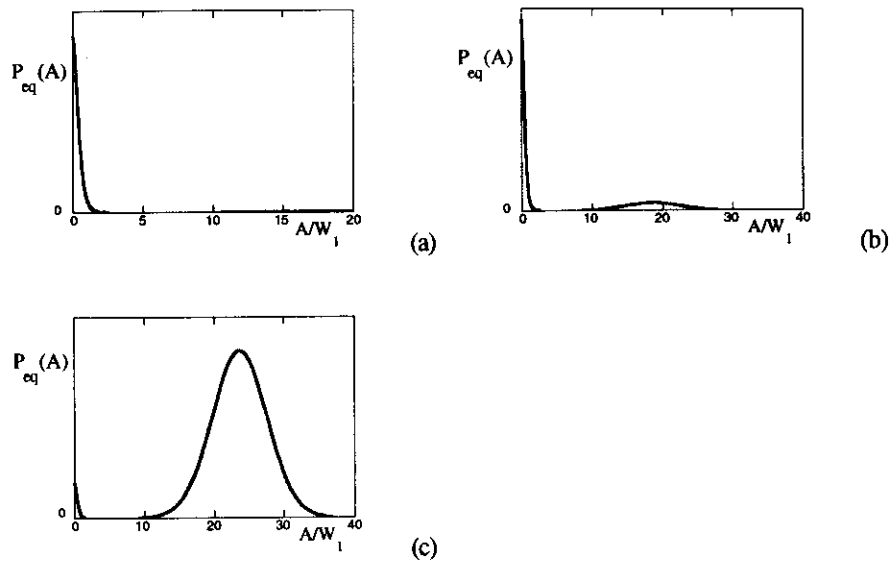

Fig.6 Typical examples of the PDF in the stationary state. The cases of (a) $\beta_p/\beta_{pc} = 1.35$ (NTM is not excited as an average), (b) $\beta_p/\beta_{pc} = 1.4$ (near marginal condition), and (c) $\beta_p/\beta_{pc} = 1.51$ (most unstable, and NTM is excited), are shown. (Other parameters are: $W_1 = W_2$, $C_1/2C_2W_1 = 1$, $hW_1 = 0$ and $\Gamma C_2 W_1 = 5$.)

separated by a local maximum at

$$A = A_m . \tag{40b}$$

Statistical transitions take place between these solutions. The dominant (i.e., the most probable) state is determined by the balance between the transition for excitation (from $A = 0$ to $A = A_s$) and the decay (from $A = A_s$ to $A = 0$). The long time average, i.e., the statistical average $\langle A \rangle$, is calculated from the PDF.

Figure 6 illustrates examples of the PDF for various cases. Fig.6(a) is the low beta case where the NTM perturbation is rarely excited and the amplitude $A \simeq 0$ holds as a statistical average. Figure 6(b) shows the intermediate case. In this case, intermittent excitation of perturbation takes place from $A = 0$ to $A = A_s$. Figure 6(c) indicates the high beta case that the state with the amplitude $A = A_s$ is the dominant solution. They are summarized in Fig.7. In the low beta case (a), the mode amplitude is low. In the case of (b), the states of $A = 0$ and $A = A_s$ are equally realized. In the high beta case (c), the state $A = A_s$ is realized as an average.

$P_{eq}(A)$ has a peak at $A = 0$. A noise level where the NTM is not excited is evaluated from a local average of A near $A = 0$, being given as

$$\langle A_0 \rangle \sim 0.5\left(-\Gamma \Delta'_0\right)^{-2/3} \tag{41}$$

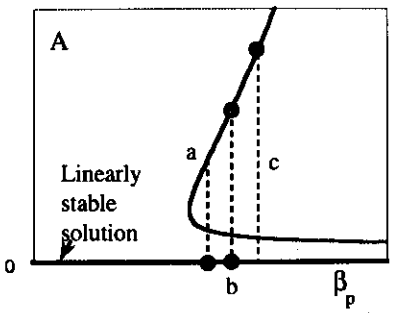

Fig.7 Schematic drawing of the long time average. a, b and c correspond to those in Fig.6, respectively.

3.3 Transition probability

Transitions between $A = 0$ and $A = A_s$ occur as is illustrated in Fig.4 owing to the random kick by noise. Calculating a flux of probability density from Fokker-Planck equation (34) [1, 30-33], the frequencies of transitions are obtained. The frequency of excitation (from $A = 0$ to $A = A_s$) and that for decay (from $A = A_s$ to $A = 0$) are expressed as

$$r_{ex} = \frac{\eta \sqrt{\Lambda_0 \Lambda_m}}{2\pi} \exp\left(-S(A_m)\right), \tag{42a}$$

$$r_{dec} = \frac{\eta \sqrt{\Lambda_s \Lambda_m}}{2\pi} \exp\left(S(A_s) - S(A_m)\right), \tag{42b}$$

respectively, where the time rates $\Lambda_{m,s}$ are given as

$$\Lambda_{m,s} = 2A \left| \partial \Lambda / \partial A \right| \text{ at } A = A_m \text{ and } A = A_s . \tag{43}$$

and

$$\Lambda_0 = \Lambda\left(\langle A_0 \rangle\right) . \tag{44}$$

Note that $\Lambda_{0,m,s}$ are normalized, being of the order unity [30].

Figure 8(a) illustrates the barrier heights $S(A_m)$ and $S(A_m) - S(A_s)$ as a function of plasma pressure for the fixed value of Δ'_0 . The coefficients $\exp\left(-S(A_m)\right)$ and $\exp\left(S(A_s) - S(A_m)\right)$, which play dominant role in determining the transition rates in Eq.(42), are shown in Fig.8(b) as a function of the pressure gradient for the fixed value of Δ'_0 . In the case of low pressure regime, the rate of back transition, r_{dec}, is much larger than the excitation rate r_{ex}. When the pressure gradient becomes higher, the state

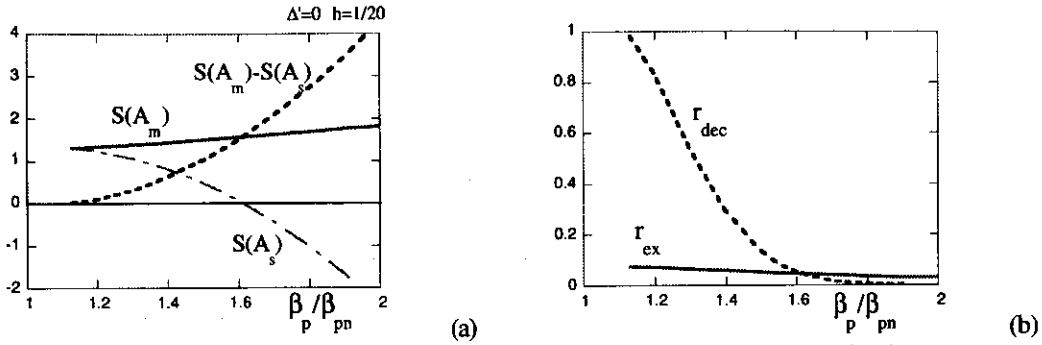

Fig.8 (a): Variation of the barrier height $S(A_m)$ and the local minimum $S(A_s)$ is shown (in the unit of ΓW_1) as a function of plasma pressure for fixed value of Δ'_0 . (b): the change of the excitation rate and decay rate for $\Gamma W_1 = 2$. r_{ex} and r_{dec} are normalized to $\eta\sqrt{\Lambda_0\Lambda_m}/2\pi$ and $\eta\sqrt{\Lambda_s\Lambda_m}/2\pi$, respectively. (Parameters are: $\Delta'_0 = 0$, $hW_1 = 1/40$, $W_1 = W_2$, $C_1/2C_2W_1 = 1$.)

$A = A_s$ turns to be a strong attractor. The excitation rate remains to be a weakly varying function in this parameter regime.

3.4 Long time average

The inverse of the transition frequency indicates the staying time. The life time being in the state $A = 0$ is given by r_{ex}^{-1} , and that in the state $A = A_s$ is given as r_{dec}^{-1} . The long time average of multiple state is given as

$$\langle A\rangle = \frac{\langle A_0\rangle r_{ex}^{-1} + A_s r_{dec}^{-1}}{r_{ex}^{-1} + r_{dec}^{-1}} \tag{45a}$$

i.e.,

$$\langle A\rangle = \left(A_s r_{ex} + \langle A_0\rangle r_{dec}\right)\left(r_{ex} + r_{dec}\right)^{-1} . \tag{45b}$$

$\langle A\rangle$ approaches to A_s if $r_{ex} > r_{dec}$ holds. It reduces to $\langle A_0\rangle$, if $r_{ex} < r_{dec}$ holds.

Figure 9 shows the statistical average $\langle A\rangle$ as a long time average, together with threshold and saturation amplitudes (A_m and A_s), as a function of β_p . Solid line shows the statistical average $\langle A\rangle$. A thin dotted line indicates the threshold A_m and saturation amplitude A_s from the deterministic model. $\langle A\rangle$ drastically changes across the condition $\beta_p = \beta_{p*}$, an approximate formula of which is derived in the next subsection.

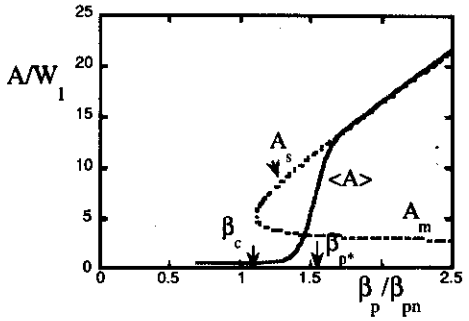

Fig.9 Amplitude of NTM as a function of the plasma pressure for fixed value of Δ'_0. Solid line shows the statistical average $\langle A \rangle$. A thin dotted line indicates the threshold A_m and saturation amplitude A_s of the deterministic model. Normalized β_p is given by Eq.(10b). (Parameters are: $\Delta'_0 = 0$, $hW_1 = 1/40$, $W_1 = W_2$, $C_1/2C_2W_1 = 1$, $\Gamma W_1 = 5$.)

It is noted that the inverse of the transition frequencies, r_{ex}^{-1} and r_{dec}^{-1}, denote the characteristic time scale by which the PDF is relaxed to $P_{eq}(A)$.

It must also be noted that the long time average in Fig.9 is a monotonous curve while the deterministic model (dotted line) predicts a multiple-valued curve. Whether a hysteresis is observed or not depends on the competition between the life time of transitions, r_{ex}^{-1} and r_{dec}^{-1}, and the characteristic time for variation of the global parameters τ_{global}. Details have been discussed in [32]. When the change of the global parameters is slow and the relation $\tau_{global} >> r_{ex}^{-1}, r_{dec}^{-1}$ holds, the value of long time average is realized. And the monotonous dependence of $\langle A \rangle$ is observed. In contrast, if the global change is fast, $\tau_{global} \sim r_{ex}^{-1}, r_{dec}^{-1}$, the hysteresis characteristics are observed.

3.5 Phase boundary

The phase boundary for the statistical average is determined by the condition

$$r_{ex} = r_{dec} . \tag{46}$$

From Eq.(42), Eq.(46) can be written as

$$S(A_s) + \frac{1}{2} \ln\left(\frac{\Lambda_s}{\Lambda_0}\right) = 0 \tag{47}$$

Apart from a logarithmic dependence, the condition is approximately given by

$$S(A_s) = 0 . \tag{48}$$

This provides the condition that global parameters must satisfy at the phase boundary. Equation (48) is investigated for two limiting cases of $h \simeq 0$ and $\Delta'_0 \simeq 0$ in the following subsections.

3.5.1 The limit where MHD nonlinear term is ineffective

When one studies the case of fairly strong linear stability, $\Delta'_0 < 0$, the MHD nonlinear stability term (with h) may be unimportant in the nonlinear potential $S(A_s)$. In this case, the condition $S(A_s) = 0$ is approximated from Eq.(37) as

$$-\frac{4}{3}\Delta'_0 A_s^{3/2} - C_2 A_s + C_1 \ln\left(A_s W_1^{-1}\right) + C_2 W_2 \ln\left(1 + A_s W_2^{-1}\right) = 0 \qquad (49)$$

where $A_s >> W_1$ is assumed. In the limit of $h = 0$, we use an approximate estimate of A_s from Eq.(18) as

$$A_s \simeq C_2^2 / 4\Delta'^2_0 , \qquad (50)$$

Substituting Eq.(50) into the first and second terms of Eq.(49), Eq.(49) is rewritten as

$$\frac{-\Delta'_0 \sqrt{W_1}}{C_2} = M \qquad (51a)$$

where

$$M = \frac{1}{\sqrt{12\left(b \ln\left(A_s W_1^{-1}\right) + W_2 W_1^{-1} \ln\left(1 + A_s W_2^{-1}\right)\right)}} \qquad (51b)$$

is a slowly varying function. Combining Eqs.(50) and (51a), one eliminates Δ'_0 from Eq.(50) and has a relation

$$A_s \simeq \frac{1}{4}\frac{W_1}{M^2} . \qquad (52)$$

Substitution of Eq.(52) into Eq.(51b) gives an equation that determines the coefficient M as

$$\frac{1}{4M^2} = 3\, b \ln\left(\frac{1}{4M^2}\right) + 3\,\frac{W_2}{W_1} \ln\left(1 + \frac{W_1}{W_2}\frac{1}{4M^2}\right) . \qquad (53a)$$

By successive substitution, one has an estimate of the solution of Eq.(53a) as

$$\frac{1}{4M^2} \simeq 3b \ln\left(3b \ln\left(3\,b\right)\right) + 3\,\frac{W_2}{W_1} \ln\left(1 + \frac{W_1}{W_2}\, 3b \ln\left(3\,b\right)\right) + \cdots , \tag{53b}$$

and the coefficient M is approximately given as

$$M = \frac{1}{\sqrt{12\left(b \ln\left(3b \ln 3b\right) + W_2 W_1^{-1} \ln\left(1 + W_1 W_2^{-1} \ln\left(3b \ln 3b\right)\right)\right)}} . \tag{53c}$$

Figure 10 shows M (the solution of Eq.(53a)) and the approximate formula Eq.(53c).

From Eq.(51a) we have the relation of the phase boundary for the statistical average as

$$\Delta'_0 = \Delta'_* \equiv -M\, W_1^{-1/2}\, C_2 , \tag{54}$$

where dominant terms are retained. The boundary Δ'_* is negative and of the order unity. Equation (54) is rewritten as

$$\Delta'_0 = \Delta'_* \equiv -M \sqrt{\frac{1}{W_1}}\, \frac{\beta_p}{\beta_{pn}} \tag{55}$$

by the help of Eq.(10a).

The phase boundary Eq.(55) is reformulated in a form of a critical pressure as

$$\beta_p = \beta_{p*} \equiv M^{-1} \sqrt{W_1}\, \beta_{pn}\left(-\Delta'_0\right) , \tag{56}$$

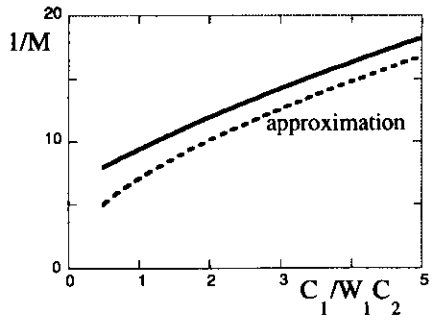

Fig.10 Coefficient M . Numerical solution (solid line) and approximate formula Eq.(53c) (dashed line) for the case of $W_1 = W_2$.

or more explicitly,

$$\beta_{p*} = \frac{1}{M} \frac{L_p}{2a_{bs}\varepsilon^{1/2}L_q}\left(-\Delta'_0\right)\frac{\rho_b}{r_s} . \tag{57}$$

Critical condition for the onset of statistical average of the perturbation follows this formula. It is found that the condition for the phase boundary β_{p*} has the same parameter dependence on the cusp point β_{pc}, Eq.(22). The numerical solution of Eq.(48) gives that β_{p*} is larger than β_{pc} by a factor which is close to unity (~ 1.5).

3.5.2 Near marginal MHD stability condition

Near the marginal stability condition of linear stability, $\Delta'_0 = 0$, the balance between the second, third and fourth terms in the RHS of Eq.(37) determines the nonlinear potential. We have an estimate from Eq.(18) as

$$A_s \simeq \frac{C_2}{2h} - W_1 + \cdots \tag{58}$$

By substituting Eq.(58) into Eq.(37), one has an estimate of $S(A_s)$ as

$$\frac{S(A_s)}{\Gamma C_2 W_1} \simeq -\frac{C_2}{4hW_1} + (2b+1)\ln\left(\frac{C_2}{2h}\right) . \tag{59}$$

The condition $S(A_s) = 0$ gives the relation

$$C_2 = (8b+4)\, W_1\, h \ln\left(\frac{C_2}{2h}\right) . \tag{60}$$

Because the logarithmic function $\ln\left(C_2/2h\right)$ is a slowly varying function, a successive substitution gives an approximate form

$$C_2 = 4(8b+4)\ln\left(4b+2\right)W_1 h , \tag{61}$$

as the condition that satisfies $S(A_s) = 0$. This equation (61) can be rewritten as

$$\beta_p = \beta_{p*} = 4(8b+4)\ln\left(4b+2\right)h\,\beta_{pn}\,W_1 . \tag{62}$$

Equation (62) shows that the critical poloidal beta value for transition β_{p*} is in proportion to W_1 , i.e.,

$$\beta_{p*} \propto \rho_b^2 r_s^{-2} . \tag{63a}$$

This must be compared to the relation for the case of strong linear stability, Eq.(57), where the scaling relation

$$\beta_{p*} \propto \rho_b r_s^{-1} \tag{63b}$$

holds. We may observe both $\rho_b r_s^{-1}$ and $\rho_b^2 r_s^{-2}$ dependencies as the phase boundary.

3.5.3 Phase boundary for the onset of NTM

Equation (48) is numerically solved, and the boundary of phase that satisfies Eq.(48) is obtained. Figure 11 shows the phase boundary β_{p*} on the (Δ'_0, β_p) plane by the solid line. Thin dashed lines in Fig.11 show the ridge points of the cusp, β_{pc}, in the deterministic model. Away from the critical point of the cusp, which is denoted by "C" in Fig.11, the boundary of phase is approximated as a straight line. Combining two limiting formulas, Eqs.(57) and (62), an analytic expression of the fitting formula of the boundary in phase space is obtained as

$$\beta_{p*} \equiv \left(M^{-1}\left(-\Delta'_0\right)\frac{\rho_b}{r_s} + 4\left(8b+4\right)\ln\left(4b+2\right)h\frac{\rho_b^2}{r_s^2} \right)\beta_{pn} . \tag{64}$$

for the case of $\Delta'_0 \leq 0$. The first and second terms in the parenthesis of Eq.(64) have dependencies $\propto \rho_b r_s^{-1}$ and $\propto \rho_b^2 r_s^{-2}$, respectively. The phase boundary for stochastic excitation of NTM is dependent on the MHD parameters Δ'_0 and h as is illustrated by Eq.(64). If the linear tearing mode is strongly stable,

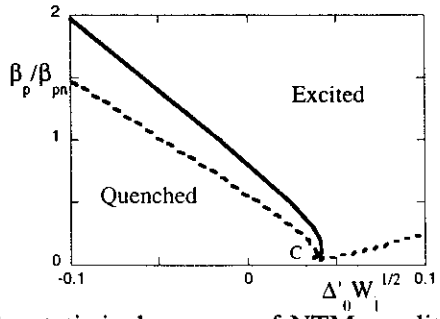

Fig.11 Phase diagram of the statistical average of NTM amplitude. In the region of "excited", the NTM is found excited after statistical average. In the region "quenched", NTM is not excited as an average. Thin dashed line is the boundary of the cusp in the deterministic model, which is shown in Fig.3(a). Symbol "C" denotes the critical point of the cusp. (Other parameters are: $hW_1 = 1/40$, $W_1 = W_2$ and $C_1/2C_2W_1 = 1$)

$$\frac{-\Delta'_0}{h}\frac{1}{4(8b+4)\ln(4b+2)M} > \frac{\rho_b}{r_s}, \tag{65a}$$

one has the linear dependence $\beta_{p*} \propto \rho_b/r_s$. On the contrary, the linear stability is weak,

$$0 < \frac{-\Delta'_0}{h}\frac{1}{4(8b+4)\ln(4b+2)M} < \frac{\rho_b}{r_s}, \tag{65b}$$

one obtains the quadratic dependence as $\beta_{p*} \propto \rho_b^2/r_s^2$.

It must also be noted that the boundary in the phase diagram does not depend on the absolute value of Γ. In other words, the boundary does not depend on the level of back-ground fluctuations.

3.6 Frequency of excitation of NTM

3.6.1 Stochastic excitation frequency

The excitation frequency r_{ex} gives the rate at which the neoclassical tearing mode is stochastically excited by the noise. This stochastic transition rate is important in experiments. The NTM is expected to appear within the characteristic time of r_{ex}^{-1}, if the parameters reaches the condition Eqs.(56) or (62). In other words, the plasma is not free from NTM in a time longer than r_{ex}^{-1}, even though the plasma condition is controlled such that the global events, which can trigger the NTM, are suppressed.

An example of the excitation frequency is estimated in the following. The height of the potential barrier $S(A_m)$ dominantly influences the rate of excitation. In the limit of small amplitude, the potential $S(A)$ is dominated by the contributions form the pressure terms. A Taylor expansion with respect to the amplitude is made as

$$S(A) = \left(\frac{C_1}{W_1^2} - \frac{C_2}{W_2}\right)\frac{A^2}{2} + \frac{C_2}{3W_2^2}A^3 - \left(\frac{C_1}{W_1^4} + \frac{C_2}{W_2^3}\right)\frac{A^4}{4} + \cdots. \tag{66}$$

The potential barrier $S(A_m)$ is given by the maximum. For the case of $W_2 > W_1$, one has a simple estimate

$$S(A_m) \simeq \left(1 - \frac{2C_2W_1^2}{C_1W_2}\right)\frac{C_1}{4} \sim \frac{C_1}{4}, \tag{67}$$

by keeping the first order correction of W_1/W_2.

It should be noted that W_1 must be finite even though the limit of small W_1 is discussed. The nonlinear potential Eq.(37) becomes divergent for $W_1 = 0$ and $\Delta'_{c2} \to \infty$, so that the barrier crossing is prohibited.

Substituting the barrier height Eq.(67) into Eq.(42a), one gets the excitation rate of NTM as

$$r_{ex} \simeq \frac{\eta \sqrt{\Lambda_0 \Lambda_m}}{2\pi} \exp\left(-\Gamma \frac{C_1}{4}\right). \tag{68}$$

3.6.2 Example

Explicit value of the transition rate is examined for a possible micromode for typical experimental parameters. The parameter Γ is the key for the transition frequency. For the L-mode plasmas, when one employs the current-diffusive ballooning mode as the micro mode, one has

$$A_h \simeq 10\, s\, \alpha^2 \left(\delta / r_s\right)^2, \tag{69a}$$

$$\phi_h \simeq 10\, \alpha^{3/2} \left(\delta / r_s\right)^2 \tag{69b}$$

and

$$\tau_{ac} \sim \alpha^{-1/2}, \tag{69c}$$

where

$$\alpha = -q^2 R \mathrm{d}\beta/\mathrm{d}r \tag{70}$$

is the normalized pressure gradient [34]. Substituting Eq.(68) into the formula of Γ, Eq.(38), one has

$$\Gamma = 2\ell k^{-3} \left(-\alpha^{-1/2}\left(1+\alpha\right) + s\sqrt{\beta m_i / m_e}\right)^{-2} 10^{-4} s^{-4} \alpha^{-11/2} R_M^{-1} \left(\delta / r_s\right)^{-8}. \tag{71}$$

The argument $\Gamma C_1/4$ in Eq.(68) may be simplified as

$$\frac{\Gamma C_1}{4} \simeq \frac{a_{bs} \varepsilon^{1/2} L_q^2}{4 \times 10^4 L_p^2 s^2} \frac{m_e}{\beta m_i} \frac{\ell}{k^3 \alpha^{11/2}} \frac{\beta_p}{R_M} \frac{\rho_b^2 r_s^6}{\delta^8} \tag{72}$$

for $\beta m_i/m_e > 1$. This result shows that when the resistivity becomes so low as to satisfy the condition

$$R_{\mathrm{M}} \simeq 10^{-4}\left(m_e/\beta m_i\right) \ell\, k^{-3}\alpha^{-11/2}\,\rho_b^2 r_s^6 \delta^{-8} \ , \tag{73}$$

the relation

$$\Gamma\, C_1/4 \sim 1 \ , \tag{74}$$

holds. That is, the exponential term increases and becomes of the order of unity, and the transition frequency of the order of η is expected.

When the plasma pressure gradient becomes large, a strong turbulence (M-mode) has been predicted [28, 35]. In this case, $\tilde{A}_h$ is enhanced by the factor of $\left(\alpha\beta_i m_i/m_e\right)^{1/2}$. One has

$$\frac{\Gamma\, C_1}{4} \simeq \frac{a_{\mathrm{bs}}\varepsilon^{1/2} L_q^2}{4\times 10^4 L_p^2 s^2}\left(\frac{m_e}{\beta m_i}\right)^3 \frac{\ell}{k^3\alpha^{15/2}} \frac{\beta_{\mathrm{p}}}{R_{\mathrm{M}}} \frac{\rho_b^2 r_s^6}{\delta^8} \ . \tag{75}$$

The condition for frequent transitions, $\Gamma\, C_1/4 \sim 1$, is given as

$$R_{\mathrm{M}} \simeq 10^{-4}\left(m_e/\beta m_i\right)^3 \ell\, k^{-3}\alpha^{-15/2}\,\rho_b^2 r_s^6 \delta^{-8} \ . \tag{76}$$

This condition can be easily satisfied in a high temperature experiment of modern tokamaks.

IV. Summary and discussions

In summary, we have developed a statistical theory for the excitation of nonlinear NTM. The stochastic equation is formulated including the presence of subcritical excitation mechanism of NTM. The rate of transition and the statistical average of amplitude are derived, and the phase boundary in plasma parameter space, $\beta_{\mathrm{p}*}$ or Δ'_*, is obtained. An analytic formula is given as Eq.(64). Linearly stable systems are prone to nonlinear instability if $S(A_{\mathrm{s}}) < 0$ holds. The formula is applied to either cases of micro fluctuations or of other random MHD activities. Empirical database for the presence of NTM must be compared with the result of phase boundary derived from the statistical theory. The rate of stochastic transition depends on the microfluctuation level and is evaluated for example cases. However, the boundary is given by $S(A_{\mathrm{s}}) = 0$ and is insensitive to the magnitude of micro fluctuations. It is plausible that the stochastic

transition without the trigger by large MHD events (e.g., sawtooth or fish-bone instabilities) can be observed in high temperature tokamak plasmas if the condition $\beta_p > \beta_{p*}$ is satisfied. This explains observations in refs.11 and 12. The dependence of β_{p*} on ρ_b/r_s is found to vary in the range between ρ_b/r_s and $(\rho_b/r_s)^2$, depending on the linear stability of the tearing mode. The empirical database has been constructed for the critical condition of the onset of tearing mode [36]. The empirical onset condition must be compared to the phase boundary. When the plasma beta value is smaller to that at the critical point of the cusp (point C in Fig.3(b) or Fig.11), the supercritical excitation of the tearing mode takes place.

From the statistical theory in this article, the observation of the hysteresis in the relation of $A(\beta_p)$ is explained. Whether a hysteresis is observed or not depends on the competition between the life times of states $A = A_s$ and $A \simeq 0$ (r_{dec}^{-1} and r_{ex}^{-1}, respectively) and the characteristic time for variation of global parameters, τ_{global}. When global parameters change slowly, i.e., $\tau_{global} >> r_{ex}^{-1}, r_{dec}^{-1}$, the long time average is realized and the monotonous dependence on the global parameters is observed. In contrast, if the parameter change is fast, $\tau_{global} \sim r_{ex}^{-1}, r_{dec}^{-1}$, the hysteresis is observed.

Equation (42) is a generalization of the result of thermal equilibrium, i.e., Eq.(496) of ref.14 that recovers Arrhenius' law, to the case of the turbulence trigger. The turbulence amplitude is included in the denominator of $S(A)$ that appears in exponential term of r_{ex} and r_{dec}. Owing to the turbulence trigger, the transition probability is greatly enhanced and the variation of the average $\langle A \rangle$ across $\beta_p = \beta_{p*}$ becomes less sharp. The energy of microfluctuations is estimated in tokamak turbulence and is about $\delta^2 r_s \lambda_D^{-3}$ times larger than that in thermal equilibrium (§23 of ref.1). For the thermal fluctuations, Γ is larger by a factor $\delta^4 r_s^2 \lambda_D^{-6}$ and the transition is very difficult to occur.

This article does not give a complete picture for the trigger of NTM but provides a theoretical framework for future studies. There are effects and contributions which should be incorporated in the nonlinear statistical theory. (Examples include: The coherent part of RHS of Eq.(23), like dynamo term and other nonlinear drags, can influence Λ so as to modify β_{p*} ; Excitation of large scale island, in turn, may suppress the transport as in the case of the Snakes phenomena [37]; Semi-micro structures could coexist as reviewed in ref.1.) The analytic formula (55) (56) and (62) could be verified by direct solution of Eq.(33) by Monte Carlo simulation. When one performs the quantitative comparison, the shift of linear stability boundary must be taken into account. The linear stability boundary of the tearing mode is modified as $\Delta_0' > \Delta_{GGJ}'$, where Δ_{GGJ}' is a positive number in the case of magnetic well [29]. If this effect is taken into account, $-\Delta_0'$ in the formula in this article is replaced by $\Delta_{GGJ}' - \Delta_0'$. It is also noted that the coefficient C_2 in Eq.(9) has a weak dependence on collisionality. If one keeps this

dependence on collisionality, the phase boundary (e.g., Eqs.(57) and (64)) has also weak dependence on the collision frequency, which is obtained by straightforward calculation. These are left for future studies and will give quantitative results.

Acknowledgements

Authors acknowledge Dr. Y. Miura and Prof. H. Zohm for useful discussions on experimental observations and Prof. M. Vlad and Prof. F. Spineanu for improving the manuscript. This work is partly supported by the Grant-in-Aid for Scientific Research of MEXT Japan and by the collaboration programs of National Institute for Fusion Science and of the Research Institute for Applied Mechanics of Kyushu University.

References

[1] A. Yoshizawa, S.-I. Itoh, K. Itoh: *Plasma and Fluid Turbulence* (IOP, England, 2002)
[2] J. A. Krommes: Phys. Reports **360** (2002) 1
[3] H. P. Furth, J. Killeen, M. N. Rosenbluth: Phys. Fluids **6** (1963) 459
[4] P. H. Rutherford: Phys. Fluids **6** (1973) 1903
[5] P. H. Rebut and M. Hugon: in *Plasma Physics and Controlled Nuclear Fusion Research 1984* (IAEA, Vienna, 1985) Vol.2, p197
[6] J. D. Callen, et al.: in *Plasma Physics and Controlled Nuclear Fusion Research* (IAEA, Vienna, 1986) Vol.2, p157
[7] A. I. Smolyakov: Plasma Phys. Contr. Fusion **35** (1993) 657
[8] Z. Chang, et al.: Phys. Rev. Lett. **74** (1995) 4663
[9] O. Sauter, et al. Phys. Plasmas **4** (1997) 1654
[10] R. J. Buttery, et al.: Plasma Phys. Contr. Fusion **42** (2000) B61
[11] A. Gude, et al.: Nucl. Fusion **39** (2001) 127
[12] A. Isayama, et al.: Nucl. Fusion **41** (2001) 761
[13] See also ITER Physics Basis: Nucl. Fusion **39** (1999) Chapter 3, Section 2.3
[14] See for a review S. Chandrasekhar: Rev. Mod. Phys. **15** (1943) 1
[15] F. Walleffe: Phys. Fluids **9** (1997) 883
[16] A. Bergmann, E. Poli, A. G. Peeters: presented at 19th IAEA Conference on Fusion Energy (2002, Lyon) paper TH/P1-01
[17] F. Waelbroeck and R. Fitzpatrick: Phys. Rev. Lett. **78** (1993) 1703; R. Fitzpatrick: Phys. Plasmas 2 (1994) 825.
[18] E. Poli, et al.: Phys. Rev. Lett. **88** (2002) 075001.
[19] H. R. Wilson, et al.: Plasma Phys. Contr. Fusion **38** (1996) A149
[20] A. B. Mikhailovskii et al.: Phys. Plasmas 7 (2000) 3474.
[21] M. Yagi, S.-I. Itoh, A. Fukuyama and K. Itoh: 7th IAEA Technical Committee Meet. H-mode Physics and Transport Barriers, Oxford, Sept 1999.
[22] A. Furuya, S.-I. Itoh, M. Yagi: J. Phys. Soc. Jpn. **70** (2001) 407;
[23] A. Furuya, S.-I. Itoh, M. Yagi: J. Phys. Soc. Jpn. **71** (2002) 1261
[24] M. Kotschenreuther, R. D. Hazeltine and P. J. Morrison: Phys. Fluids **28** (1990) 779.
[25] J. A. Wesson: *Tokamaks* (Oxford, 1987) Section 7.3
[26] S.-I. Itoh, K. Itoh, M. Yagi: Phys. Rev. Lett. **91** (2003) 045003.
[27] M. Yagi, et al.: Plasma Phys. Contr. Fusion **39** (1997) 1887
[28] K. Itoh, S.-I. Itoh and A. Fukuyama: *Transport and Structural Formation in Plasmas* (IOP, England, 1999)
[29] A. H. Glasser, J. M. Greene, J. L. Johnson, Phys. Fluids **18** (1975) 875
[30] S.-I. Itoh and K. Itoh: J. Phys. Soc. Jpn. **69** (2000) 427
[31] S.-I. Itoh, K. Itoh, S. Toda: Phys. Rev. Lett. **89** (2002) 215001
[32] S.-I. Itoh, K. Itoh and S. Toda: Plasma Phys. Control. Fusion **45** (2003) 823
[33] K. Itoh, S.-I. Itoh, F. Spineanu, M. O. Vlad and M. Kawasaki: Plasma Phys. Control. Fusion **45** (2003) 911
[34] A. Fukuyama, et al.: Plasma Phys. Control. Fusion **37** (1995) 611
[35] S.-I. Itoh, et al.: Plasma Phys. Contr. Fusion **38** (1996) 527
[36] H. Zohm et al., in Proc. 18th IAEA Conference on Fusion Energy (Sorrento, 2000) paper IAEA-CN-77/EX3/1.
[37] A. Weller et al.: Phys. Rev. Lett. **59** (1987) 2303

Recent Issues of NIFS Series

NIFS-760 T. Hayashi, N. Mizuguchi, H. Miura, R. Kanno, N. Nakajima and M. Okamoto
Nonlinear MHD Simulations of Spherical Tokamak and Helical Plasmas
Oct. 2002 (TH/6-3)

NIFS-761 K. Yamazaki, S. Imagawa, T. Muroga, A. Sagara, S. Okamura
System Assessment of Helical Reactors in Comparison with Tokamaks
Oct. 2002 (FT/P1-20)

NIFS-762 S. Okamura, K. Matsuoka, S. Nishimura, M. Isobe, C. Suzuki, A. Shimizu, K. Ida, A. Fujisawa, S. Murakami, M. Yokoyama, K. Itoh, T. Hayashi, N. Nakajima, H. Sugama, M. Wakatani, Y. Nakamura, W. Anthony Cooper
Physics Design of Quasi-Axisymmetric Stellarator CHS-qa
Oct. 2002 (IC/P-07)

NIFS-763 Lj. Nikolic, M.M. Skoric, S. Ishiguro and T. Sato
On Stimulated Scattering of Laser Light in Inertial Fusion Energy Targets
Nov. 2002

NIFS-764
NIFS Contributions to 19th IAEA Fusion Energy Conference (Lyon, France, 14-19 October 2002)
Nov. 2002

NIFS-765 S. Goto and S. Kida
Enhanced Stretching of Material Lines by Antiparallel Vortex Pairs in Turbulence
Dec. 2002

NIFS-766 M. Okamoto, A.A. Maluckov, S. Satake, N. Nakajima and H. Sugama
Transport and Radial Electric Field in Torus Plasmas
Dec. 2002

NIFS-767 R. Kanno, N. Nakajima, M. Okamoto and T. Hayashi
Computational Study of Three Dimensional MHD Equilibrium with m/n=1/1 Island
Dec. 2002

NIFS-768 M. Yagi, S.-I. Itoh, M. Kawasaki, K. Itoh and A. Fukuyama
Multiple-Scale Turbulence and Bifurcaion
Jan. 2003

NIFS-769 S.-I. Itoh, K. Itoh and S. Toda
Statistical Theory of L-H Transition and its Implication to Threshold Database
Jan. 2003

NIFS-770 K. Itoh
Summary: Theory of Magnetic Confinement
Jan. 2003

NIFS-771 S.-I. Itoh, K. Itoh and S. Toda
Statistical Theory of L-H Transition in Tokamaks
Jan. 2003

NIFS-772 M. Stepic, L. Hadzievski and M.M. Skoric
Modulation Instability in Two-dimensional Nonlinear Schrodinger Lattice Models with Dispersion and Long-range Interactions
Jan. 2003

NIFS-773 M.Yu. Isaev, K.Y. Watanabe, M. Yokoyama and K. Yamazaki
The Effect of Hexapole and Vertical Fields on α-particle Confinement in Heliotron Configurations
Mar. 2003

NIFS-774 K. Itoh, S.-I. Itoh, F. Spineanu, M.O. Vlad and M. Kawasaki
On Transition in Plasma Turbulence with Multiple Scale Lengths
May 2003

NIFS-775 M. Vlad, F. Spineanu, K. Itoh, S.-I. Itoh
Intermittent and Global Transitions in Plasma Turbulence
July 2003

NIFS-776 Y. Kondoh, M. Kondo, K. Shimoda, T. Takahashi and K. Osuga
Innovative Direct Energy Conversion Systems from Fusion Output Thermal Power to the Electrical One with the Use of Electronic Adiabatic Processes of Electron Fluid in Solid Conductors.
July 2003

NIFS-777 S.-I. Itoh, K. Itoh and M. Yagi
A Novel Turbulence Trigger for Neoclassical Tearing Modes in Tokamaks
July 2003

NIFS-778 T. Utsumi, J. Koga, T. Yabe, Y. Ogata, E. Matsunaga, T. Aoki and M. Sekine
Basis Set Approach in the Constrained Interpolation Profile Method
July 2003

NIFS-779 Oleg I. Tolstikhin and C. Namba
CTBC A Program to Solve the Collinear Three-Body Coulomb Problem: Bound States and Scattering Below the Three-Body Disintegration Threshold
Aug. 2003

NIFS-780
Contributions to 30th European Physical Society Conference
on Controlled Fusion and Plasma Physics
(St.Petersburg, Russia, 7-11 July 2003)
from NIFS
Aug. 2003

NIFS-781 Ya. I. Kolesnichenko, K. Yamazaki, S. Yamamoto, V.V. Lutsenko, N. Nakajima, Y. Narushima, K. Toi, Yu. V. Yakovenko
Interplay of Energetic Ions and Alfvén Modes in Helical Plasmas
Aug. 2003

NIFS-782 S.-I. Itoh, K. Itoh and M. Yagi
Turbulence Trigger for Neoclassical Tearing Modes in Tokamaks
Sep. 2003